Zhang C, Steele TC, Wiebe LDA. 2018. Design-level estimation of seismic displacements for self-centering SDOF systems on stiff soil. *Engineering Structures*, 177: 431-443.

This material may be found at DOI 10.1016/j.engstruct.2018.09.067.

Design-level estimation of seismic displacements for self-centering SDOF systems on stiff soil

Changxuan Zhang, Taylor C. Steele, Lydell D.A. Wiebe*

Department of Civil Engineering, McMaster University, 1280 Main St. West, Hamilton ON, L8S 4L7, Canada.

Abstract

Self-centering systems, which are intended to survive a major earthquake with essentially no residual displacements, are drawing increasing attention from designers. Both force-based and displacement-based design methodologies require an estimate of the peak seismic displacements. Therefore, this study focuses on estimating the peak displacements of self-centering systems based on constant-strength (C_R) displacement demand spectra, which are calculated from more than five million nonlinear time history analyses of single-degree-of-freedom (SDOF) systems using ground motions representing a site with stiff soil conditions. Because of the ability of self-centering systems to achieve large displacement capacities while also being relatively stiff in the linear range, this study includes much lower linear limits than are used to design traditional yielding systems. Self-centering systems are shown to have displacements that are generally larger than for corresponding elastic systems, and although supplemental energy dissipation decreases the peak displacements, the influence of increasing the energy dissipation ratio, β, decreases as β approaches 100%. The secondary stiffness has relatively little influence if it is positive and small, but a negative secondary stiffness can lead to unbounded response. Using a tangent stiffness proportional damping model instead of an initial stiffness proportional damping model increases the peak displacements and makes the results more sensitive to the energy dissipation and secondary stiffness. Regression analysis is used to develop a simple equation that can be used during design to estimate the displacement demands on self-centering systems. This equation is shown to achieve a reasonable balance between simplicity and accuracy for

*Corresponding author. Tel.: +1 905 5259140 ext. 24620

Email addresses: changxuanzhang@gmail.com (Changxuan Zhang), steeletc@mcmaster.ca (Taylor C. Steele), wiebel@mcmaster.ca (Lydell D.A. Wiebe)

the design of four controlled rocking steel braced frames with heights between three and nine storeys.

Keywords: self-centering systems; nonlinear displacement ratios; constant-strength spectra; inherent damping models; controlled rocking steel braced frames

---

1. Introduction

Most modern seismic design is based on intentionally designing an inelastic deformation mechanism that involves yielding of certain elements. Those members are designed to exhibit a stable hysteretic response that limits seismic forces and dissipates energy, while other parts of the structure are capacity designed to remain elastic. The objective is that structural collapse is prevented and people can be evacuated safely after a major earthquake event. This design philosophy has proved to meet these objectives in recent earthquake events [1, 2]. Nevertheless, even if structures do not collapse, there can still be large inelastic deformations that are associated with structural damage and residual displacements. The structural damage may need repair afterwards, and the residual displacements have a strong influence on the possibility and cost of repair [3, 4].

To avoid structural damage and residual deformations, self-centering systems are drawing increasing attention. A self-centering system also has a nonlinear mechanism that limits seismic forces for capacity design, but after a major earthquake, a self-centering system returns to an essentially undeformed position without significant residual displacements. This self-centering mechanism can be achieved in many ways, including unbonded post-tensioned precast concrete moment frames [5] (Figure 1(a)) and walls [6] (Figure 1(b)), controlled rocking steel braced frames [7, 8, 9, 10] (Figure 1(c)) and self-centering energy dissipative braces [11, 12] (Figure 1(d)). While all of these self-centering systems have different mechanisms, their force-displacement relationships can all be idealized as a flag-shaped hysteresis (Figure 1(e)) with properties (initial stiffness k_1, linear limit f_y, energy dissipation parameter β, secondary stiffness k_2) that must be selected by the designer. For all the systems identified above, the characteristic flag-shaped hysteresis is generally achieved by including pre-stressed

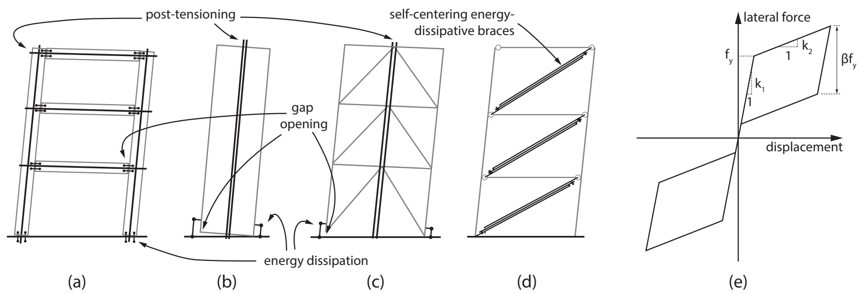

Figure 1: Self-centering systems: (a) unbonded post-tensioned concrete moment frame; (b) controlled rocking precast concrete wall; (c) controlled rocking steel braced frame; (d) steel frame with self-centering energy dissipative braces; (e) resulting flag-shaped hysteresis

post-tensioning strands to pull the system to its original position, in combination with frictional or fuse yielding energy dissipating components to provide hysteretic energy dissipation. If the restoring force provided by the post-tensioning prestress is greater than the resistance provided by the energy dissipating interface, the system will return to a plumb position with little to no residual drift. A flag-shaped hysteresis can also be obtained on a material level by using shape memory alloys (e.g. [13]). A design method for controlled rocking steel braced frames was recently proposed that is based on selecting these properties to achieve a set displacement target in an equivalent self-centering SDOF system [14]. Similarly, in conventional force-based design, the displacement must be checked against codified limits. Regardless of the selected self-centering system or the design method, the designer must be able to predict the peak displacement of the self-centering system being designed.

Christopoulos et al. [15] studied the ductility demands of self-centering SDOF systems and concluded that self-centering systems can achieve similar or reduced ductility demands compared to traditional elastoplastic systems. Seo and Sause [16] also studied displacement ductility of self-centering SDOF systems, using both an initial frequency proportional damping model and a secant frequency proportional damping model. They found that self-centering systems have higher ductility demands than elastoplastic and stiffness degrading systems when using the same response modification coefficient, R, and secondary stiffness ratio, $\alpha = k_2/k_1$, particularly when the hysteretic energy dissipation ratio is small, but can achieve similar ductility demands by combining different secondary stiffness ratios and hysteretic energy dissipation ratios. A regression equation for displacements was proposed by Seo [17] and calibrated for $R = 1.5$ to $R = 8$ and initial or secant stiffness proportional damping. Alternative regression equations have also been proposed by Rahgozar et al. [18] and by Joo et al. [19]. All of these studies have considered the linear limit of self-centering systems at similar levels to conventional yielding systems (response modification coefficients of no more than $R = 10$). However, self-centering systems have an apparent ductility that can be controlled by the designer with much more freedom than is possible with conventional yielding systems, which are limited by the material ductility capacity. In this respect, many self-centering systems have more in common with base isolation systems, for which normalizing the displacement capacity by the maximum linear displacement would result in a very large apparent ductility ratio. The nonlinear displacement and ductility demands are not associated with structural damage in self-centering systems at the design level. Therefore, higher force reduction factors may be used to reduce the quantity of post-tensioning or energy dissipating components that control the hysteretic response while still limiting seismic displacements to the same limits as are used for conventional systems [14]. While these displacements limits are not as critical for limiting material ductility demands in the lateral force resisting system, they are still important considerations for gravity framing and nonstructural component safety limits. Moreover, none of the previous studies have considered the effect of a negative secondary stiffness caused by significant P-Delta effect, nor have they investigated the peak displacements when using a tangent stiffness proportional damping model, which some studies have suggested is more realistic [20, 21].

If self-centering systems are to be included in future codes and standards in a similar manner to conventional seismic force resisting systems, it will be necessary to specify appropriate seismic performance factors, including the response modification coefficient, R, and the deflection amplification factor, C_d, which is the ratio of the nonlinear displacements in a structure to the linear displacements calculated under the reduced seismic forces. As part of this development, SDOF analyses are useful in identifying the likely range of hysteretic properties that could be considered for the design of self-centering systems, as well as approximating the peak seismic displacements of these systems without more computationally expensive multi-degree-of-freedom nonlinear time history analyses. Therefore, the main purpose of this paper is to extend the previous studies on self-centering SDOF systems to consider the influence of large response modification coefficients, negative secondary stiffness, and a tangent stiffness proportional damping model, as well as to provide an equation to estimate the displacement demands in self-centering SDOF systems with this wider range of parameters. First, the parameters used for the parametric study are introduced, and a suite of 80 ground motions representing a site with stiff soil conditions (i.e. ASCE 7 site class D [22]) is used to complete 5,529,600 nonlinear time history analyses of self-centering SDOF systems. Then, the analysis results are used to calibrate a regression equation to estimate the nonlinear displacement demands in self-centering systems for two different damping models. Finally, the regression equation is used to estimate the peak seismic displacements in four example structures that are located in the western United States and for which R and k_2 are outside the range of previous studies, and the predictions are verified by nonlinear time history analysis of the example frames.

2. Definition of parameters

The equation of motion governing the dynamic response of nonlinear SDOF systems is:

$$m\ddot{u} + c\dot{u} + f_s(u) = -m\ddot{u}_g \quad (1)$$

where m is the mass of the system; c is the viscous damping coefficient of the system; f_s is the structural force of the system; $\ddot{u}$, $\dot{u}$, and u are the relative acceleration, velocity and displacement of the system, respectively, and $\ddot{u}_g$ is the ground acceleration. In this study, m is taken as 1 kg without loss of generality.

For SDOF systems, c is related to the stiffness of the system as:

$$c = 2\zeta\sqrt{km} \quad (2)$$

where ζ is the inherent damping ratio, defined as 5% throughout this study. In this paper, when the stiffness term k_1 is used in in Equation (2) to calculate a value for c that is constant during the nonlinear time history analysis, this initial stiffness proportional damping model is referred to as the initial damping model. Most previous studies on SDOF systems have used the initial damping model (e.g. [15, 23]). In addition, a constant damping model is consistent with the mass-proportional term of a Rayleigh damping model for a multi-degree-of-freedom system. This term normally provides most of the damping in the first mode, which dominates the seismic displacements [24].

Despite the common use of the initial damping model, some researchers have concluded that this model can result in a fictitious high damping force when the stiffness of the nonlinear system reduces [16, 20, 21]. Priestley and Grant [20] suggested that a tangent stiffness proportional damping model is more realistic. Therefore, in order to identify the significance of the assumed inherent damping model, this study also includes a separate set of analyses using the tangent stiffness proportional damping model, which is defined here as:

$$c_i = \begin{cases} 2\zeta\sqrt{mk_{i-1}} & \text{if } k_{i-1} \geq 0, \\ 0 & \text{if } k_{i-1} < 0. \end{cases} \tag{3}$$

where k_{i-1} is the stiffness of the system at the end of the previous time step. This stiffness is used instead of the current stiffness to avoid convergence problems caused by iterating the stiffness within one time step. For brevity, the damping model defined by Equation (3) will be called the tangent damping model.

There is limited experimental evidence available to validate inherent damping models for self-centering systems. Rayleigh damping of 2% at the first-mode period and at five times that period was found to be the most consistently accurate model for large-scale shake table tests of an eight-storey controlled rocking steel braced frame [25]. Although the tangent stiffness matrix was used to define the damping, the damping matrix c was essentially constant because all elements that were used to calculate the damping matrix were linear elastic. The question of how best to model inherent damping for self-centering systems is outside the scope of this study. Rather, this research focuses on how the displacement demands of self-centering SDOF systems will change, and whether the trends of displacement demands with respect to different hysteretic parameters will change, if the tangent damping model is used instead of the initial damping model.

In Equation (1), the $f_s(u)$ term is related to the flag-shaped hysteresis defined by the initial stiffness, k_1, linear limit, f_y, energy dissipation parameter, β, and secondary stiffness, k_2. To normalize the results, k_1 is defined based on the initial period, T_1:

$$k_1 = 4\pi^2 \frac{m}{{T_1}^2} \tag{4}$$

The linear limit f_y is determined from f_e, the absolute peak force that a linear elastic system with the same T_1 experiences during the same earthquake record, and the response modification coefficient R:

$$f_y = \frac{f_e}{R} \tag{5}$$

In this study, values of R are chosen to go well beyond the limits of the most ductile seismic force resisting systems that are currently codified ($R = 8$) [22], up to one value of R beyond the point where wind is likely to govern over seismic loads (R =30 for the example structures shown later).

The secondary stiffness k_2 is defined in terms of the secondary period, which is analogous to the initial period but using the secondary stiffness:

$$k_2 = 4\pi^2 \frac{m}{{T_2}^2} \operatorname{sgn}(T_2) \tag{6}$$

By this definition, $k_2 < 0$ if the secondary period is negative, and systems with $T_2 = \infty$ have zero secondary stiffness. This definition avoids normalizing the secondary stiffness by the initial stiffness, thus making it possible to evaluate the influence of each stiffness independently. This is of value because the secondary stiffness of each self-centering system in Figure 1 is determined primarily by the post-tensioning properties, which have almost no effect on the initial stiffness.

The parameters considered in this study are summarized in Table 1. All of the results in this paper are obtained by programs written in MATLAB [26]. The linear and nonlinear time history analyses are carried out using Newmark's method with the unconditionally stable constant average acceleration assumption and Newton-Raphson iteration [27] with a convergence tolerance for iterated forces of 10^{-3} N, which was

Table 1: Parameters considered in SDOF analyses

System Parameter	Considered Values
Initial period, T_1	0.05 - 1.0 s (increments of 0.05 s) 1.0 - 3.0 s (increments of 0.1 s)
Secondary period, T_2	-5 s, -10 s, -20 s, ∞, 20 s, 10 s, 8 s, 5 s, 3 s, 2 s, 1.5 s, 1 s
Response modification coefficient, R	2, 4, 6, 8, 10, 15, 20, 30, 50
Hysteretic energy dissipation ratio, β	0%, 10%, 20%, 40%, 50%, 60%, 80%, 100%
Damping ratio, ζ	Initial damping model: 5% Tangent damping model: 5%

found to result in peak displacements that were within 0.01 mm of those determined using a smaller convergence criterion. The time step for elastic and nonlinear time history analyses was selected as Δt = 0.001 s based on sensitivity analysis. The sensitivity analyses are not presented here for brevity, but this time step is one fifth of the smallest time step used in previous studies on self-centering SDOF systems, and reducing the time step further did not change the peak displacements by more than 0.1% More detailed model validation is provided by Zhang [28].

3. Ground motion records and example analysis

80 unscaled broadband historical ground motion records are used for the analyses of this study. These records were selected for stiff soil sites assuming $V_{s,30}$ = 250 m/s (i.e. ASCE 7 site class D [22]) and are given as set #1A for the PEER transportation research program [29]. They are intended to represent the dominant hazard in active seismic regions with large earthquakes (M = 7) at short distances (10 km). The elastic acceleration response spectra are shown in Figure 2(a). A sample ground motion that is close to the median response spectrum is highlighted here and is used in the following example analysis.

Figure 2(b) shows the results of time history analyses with the sample ground motion and 5% inherent damping for an SDOF elastic system with T_1 = 0.5 s, and for a self-centering SDOF system with T_1 = 0.5 s, R = 8, β = 50%, and $T_2 = \infty$. In this case, the self-centering system experiences a period elongation and a larger displace-

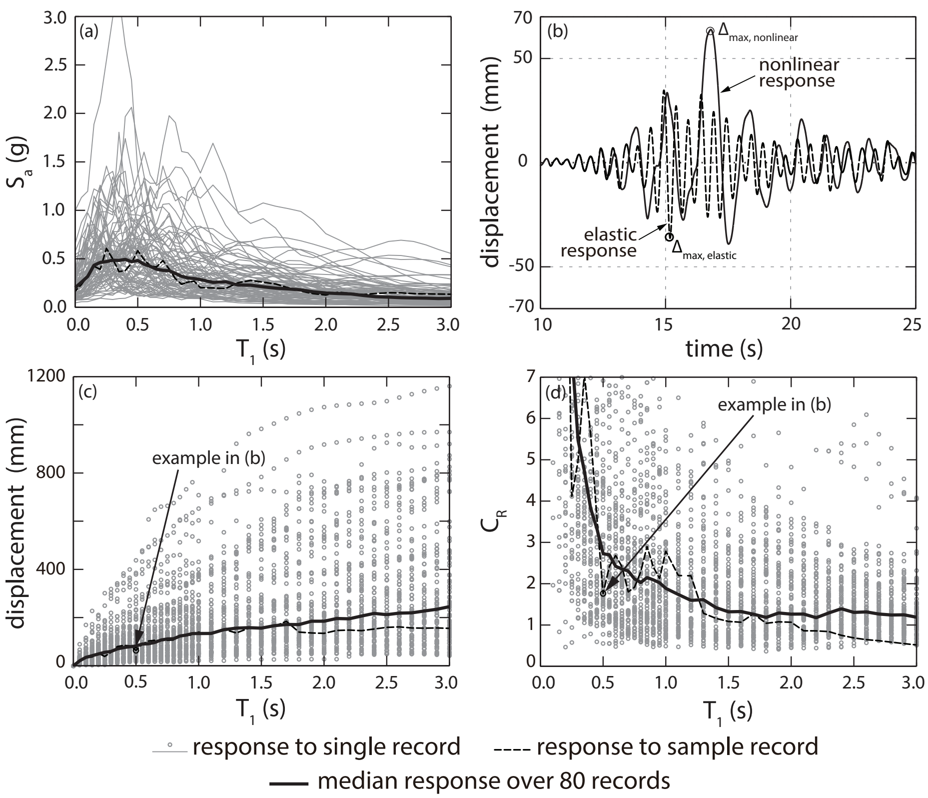

Figure 2: Broadband ground motions considered and example analysis: (a) 5% damped elastic acceleration response spectra, (b) time history analyses with sample ground motion, (c) individual and median peak displacements of self-centering SDOF systems, (d) individual and median displacement ratios of self-centering SDOF systems.

ment than the corresponding elastic system. Figure 2(c) shows the peak displacements for all 80 ground motions and for all self-centering SDOF systems with T_1 between 0.05 and 3.0 s and the same values of R, β, and T_2. Like an elastic system, the median displacements of self-centering systems increase as the initial period increases. In Figure 2(d), peak displacements of the self-centering systems are normalized by the peak displacements of corresponding elastic systems with the same initial period. This defines a constant-strength displacement demand spectrum, in which the ratio of the peak nonlinear displacement to the peak displacement of the corresponding elastic SDOF system is defined as the displacement ratio C_R:

$$C_R = \left| \frac{\Delta_{max,nonlinear}}{\Delta_{max,linear}} \right| \tag{7}$$

In this study, because the linear limit (f_y) for each nonlinear time history analysis is defined as the peak elastic force demand for that record divided by R, and the final results are expressed in terms of C_R, the ground motion scaling has the same effect on both the demand and the capacity and therefore no effect on the normalized results of C_R. For example, scaling a ground motion by a factor of 2 will increase both the elastic displacement and the nonlinear displacement by a factor of exactly 2. Therefore, when the results are normalized by the elastic displacement, the ratio is not influenced by the ground motion scaling.

The historical records used for the study were pre-processed to have a usable bandwidth of 0.01 to 10 s [30, 31]. Seo [17] showed that the response can be underestimated if the ground motion filtering removes energy content below the secant period of the system. Therefore, since it is not known whether there is significant energy content beyond the 10 s cutoff of the ground motion filter, the following results identify where the secant period exceeds 10 s. Based on the geometry of the hysteresis, the secant stiffness is calculated as:

$$k_{secant} = k_2 + (\Delta_y/\Delta_{max})(k_1 - k_2) \tag{8}$$

where Δ_y is the yield displacement, and Δ_{max} is the peak displacement reached by the system. Taking $T_{secant} = 2\pi\sqrt{m/k_{secant}}$ and replacing Δ_y/Δ_{max} with $1/(C_R R)$, Equation (8) can be rearranged to calculate C_R values that correspond to a specific secant stiffness:

$$C_R = \frac{1}{R} \times \frac{\left(\frac{1}{T_1}\right)^2 - \left(\frac{1}{T_2}\right)^2 \mathrm{sgn}(T_2)}{\left(\frac{1}{T_{secant}}\right)^2 - \left(\frac{1}{T_2}\right)^2 \mathrm{sgn}(T_2)} \tag{9}$$

Values of C_R that cause T_{secant} to be greater than 10 s are identified in Figures 3-10 and discussed in the sections below.

4. Results of the parametric study: Initial damping model

4.1. Influence of initial period

To investigate the influence of initial period, the secondary period is fixed as $T_2 = \infty$ (zero secondary stiffness) and the median values of C_R are shown with respect to T_1 in Figure 3. The values of C_R are generally significantly greater than 1.0, even for $\beta = 100\%$. This highlights the need to quantify the increased displacements of self-centering systems relative to the equal displacement assumption that is common in design. In general, C_R decreases as T_1 increases. For the case of $R = 2$ or $R = 4$, C_R becomes close to constant when $T_1 \geq 1.0$ s. However, for larger R values ($R > 8$), C_R continues to decrease with increasing T_1. The effect of the linear limit is more pronounced at short initial periods, where C_R becomes very large. For example, in the case of $\beta = 50\%$ and $T_1 = 0.1$ s, $C_R = 6.8$ when $R = 2$, $C_R = 30$ when $R = 4$, and $C_R = 41$ when $R = 8$. Although the displacement ratio of $C_R = 41$ seems very large, it corresponds to a displacement of 34 mm for a 3.5 m tall one-storey structure, or only 1% interstorey drift. The ductility demand in this case is larger than would be acceptable for conventional systems, but because this nonlinear displacement is not the result of any structural damage, this would generally be considered acceptable for a self-centering system. Reducing the linear limit can approximately double the peak displacement when the response modification coefficient is small ($R \leq 8$), but the peak displacements become less sensitive to the linear limit when the response modification

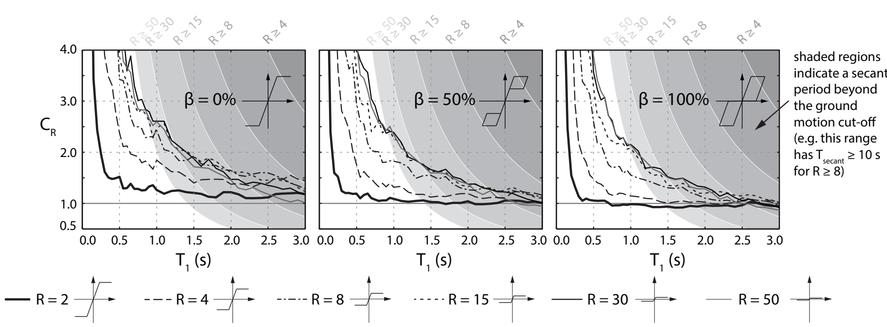

Figure 3: Displacement ratios of self-centering SDOF systems with respect to initial period with initial damping model and $T_2 = \infty$.

coefficient is already greater than about $R = 10$. Figure 3 shows that $R = 50$ can sometimes result in similar or smaller displacement demands compared to $R = 30$, even when T_{secant} using the median peak displacement is less than the cut-off period of the ground motion filter.

The shaded regions indicate the values of C_R that would cause the secant period of the structure to exceed 10 s for the different values of R. If there was significant energy content beyond 10 s, it would have been filtered out during ground motion processing, leading the an underestimate of the displacements in the shaded range. For $R \leq 8$, all of the results have secant periods within the range where the ground motions have not been filtered, while the results for $R = 15$, $R = 30$ and $R = 50$ are in this range only for initial periods shorter than $T_1 = 2.1$ s, $T_1 = 1.3$ s, and $T_1 = 0.8$ s, respectively. The cut-off points shift towards larger periods as the secondary stiffness increases, as shown later.

4.2. Influence of response modification coefficient

The variation of C_R with respect to R for different combinations of T_1 and T_2 is shown in Figure 4. C_R generally increases with increasing R for systems with different parameters. However, above a critical R value, typically in the range of 15 to 20, C_R stays constant and even decreases in some cases, although the decreases are usually observed in cases where the secant period of the system exceeds the cut-off period of the ground motion filter. Comparing different rows shows that the influence of R diminishes as T_1 becomes longer. For example, in the case of $T_1 = 0.2$ s, $T_2 = 20$ s, and $\beta = 100\%$, C_R changes from 2 to 12 when R is increased from 2 to 20. However, if $T_1 = 2.0$ s with the same T_2 and β, C_R only increases from 0.96 to 1.26 when R is increased from 2 to 20. The trends in C_R with varying R values are generally similar regardless of β.

4.3. Influence of hysteretic energy dissipation

The energy dissipation parameter β defines the hysteretic energy dissipation that is added to the assumed inherent viscous damping. The changes of C_R with respect to β are shown in Figure 5. Generally, C_R decreases as β is increased. Increasing

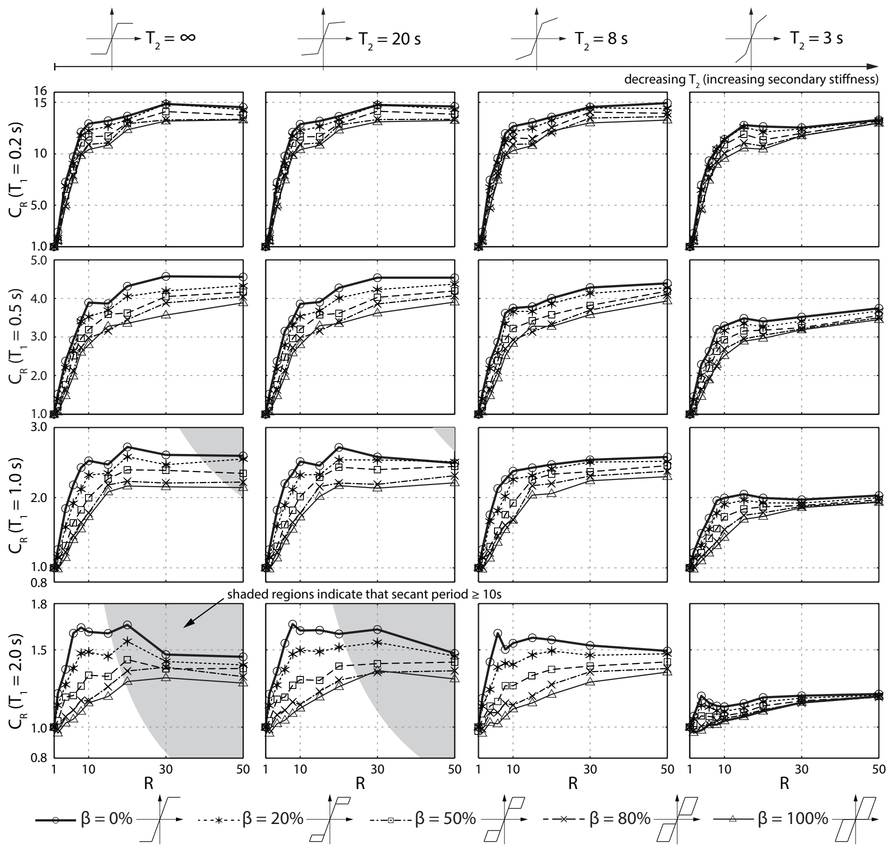

Figure 4: Displacement ratios of self-centering SDOF systems with respect to response modification coefficient with initial damping model

the hysteretic energy dissipation generally reduces the peak displacements by up to 50% when comparing the case of maximum self-centering hysteretic energy dissipation (β = 100%) to that of no hysteretic energy dissipation (β = 0%), but the curve becomes less steep as β becomes larger. This shows that there are diminishing returns with increasing β: the influence of increasing β decreases as β approaches 100%. For example, when $T_1 = 1.0$ s, $T_2 = \infty$ and $R = 8$, increasing β from 0% to 50% decreases C_R from 2.4 to 1.8, but further increasing β to 100% only decreases C_R to 1.6. Also, the energy dissipation parameter affects systems with short periods more than systems with long periods, as is clear from the limits of the y-axes in Figure 5.

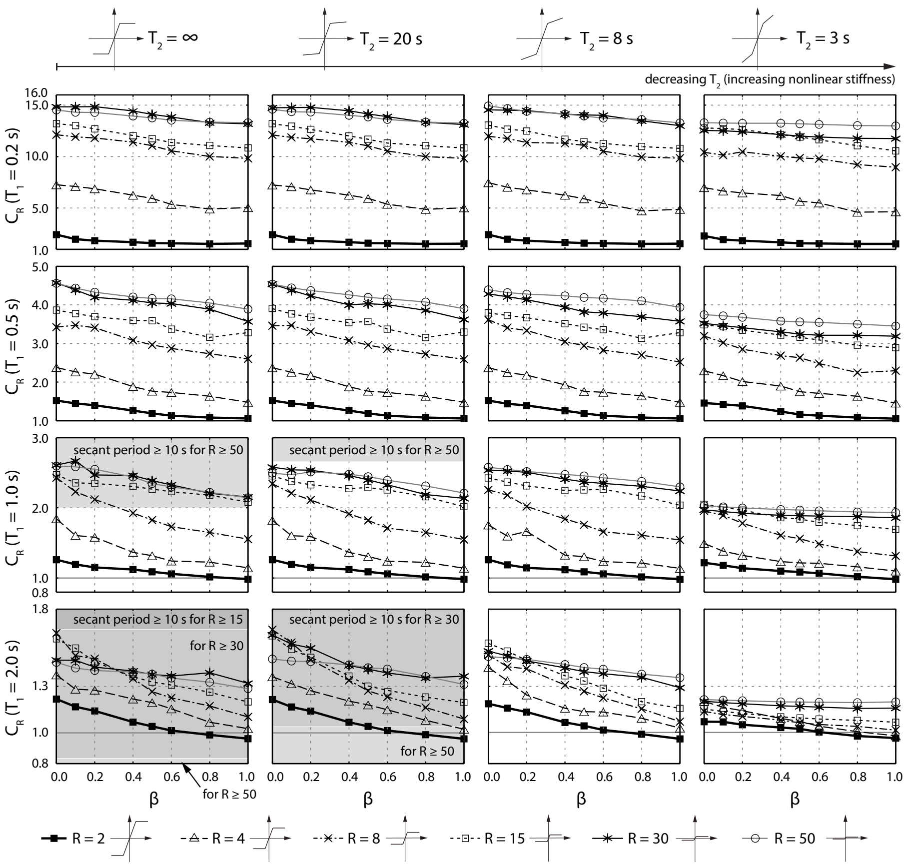

Figure 5: Displacement ratios of self-centering SDOF systems with respect to hysteretic energy dissipation parameter with initial damping model

4.4. *Influence of secondary period*

Figure 6 shows the variation of C_R with respect to T_2. Generally, when $T_2 > 0$, C_R decreases as T_2 decreases. Referring to Figure 1, the physical meaning of this is that adding post-tensioning stiffness reduces the displacement of a self-centering system. However, T_2 cannot be shorter than T_1, and practical construction limitations make it difficult for T_2 to be very close to T_1. In Figure 6 for 5 s $\leq T_2 \leq \infty$, the changes of C_R for most systems are mostly within 10%. For example, when T_1 = 0.5 s, R = 8 and β = 20%, C_R decreases from 2.1 to 2.0 when T_2 decreases from ∞ to 5 s. Exceptions are some cases where β = 0% or R = 30. For the cases where β = 0%, the secondary period has a bigger influence than for $\beta > 0\%$. For smaller values of T_2 (i.e. $T_2 < 5$ s), the displacement ratio reduces more significantly.

When T_2 becomes negative and shorter, C_R starts increasing rapidly and sometimes becomes a vertical line ($C_R \rightarrow \infty$) in Figure 6. When there is a vertical line in Figure 6, it is not because the elastic displacement is very small, since this effect has already been indicated by the larger scale of the axis for short-period structures. Rather, a vertical line means that the system experiences large nonlinear displacements in more than 50% of cases and becomes dynamically unstable. At short initial periods, dynamic instability only occurs when R is extremely large ($R = 30$ in Figure 6 where $C_R \geq 10^3$) with negative T_2. For longer initial periods, dynamic instability occurs at a smaller value of R and a negative value of T_2 that is closer to ∞. This unbounded mechanism can be physically described as representing sidesway collapse of a building structure, and it occurs when the force-displacement response crosses the zero-force line while the displacement still has a tendency of increasing. While this dynamic instability is caused by T_{secant} becoming infinite and therefore is always within the shaded region, this large displacement is a result of an unbounded response in a single direction, rather than an oscillating response with a large secant period. When the absolute value of a negative T_2 decreases, it means that the nonlinear slope is steeper so that the system is more likely to cross the zero-force line with an unbounded response. A larger R value or a longer initial period means a smaller linear limit, which also increases the likelihood of the force-displacement response of the system becoming unbounded in its nonlinear range. Thus, a combination of large R with a negative T_2 may not provide adequate dynamic stability to limit lateral displacements in self-centering systems. Previous research on conventional systems with an elastoplastic hysteresis or a hysteresis that captured strength degradation reached similar conclusions [32]. While increasing the hysteretic energy dissipation has been shown above to reduce the displacement demands in self-centering systems, increasing hysteretic energy dissipation generally cannot prevent this dynamic instability caused by negative secondary stiffness.

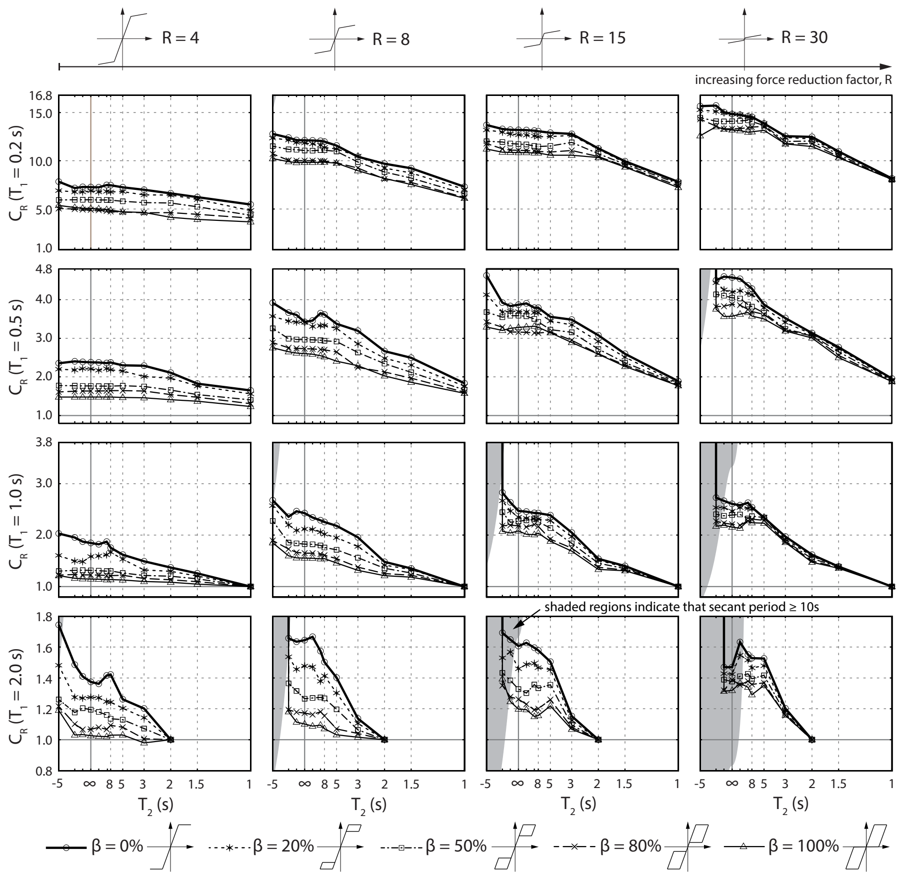

Figure 6: Displacement ratios of self-centering SDOF system with respect to secondary period with initial damping model

5. Results of the parametric study: Tangent damping model

With an intial stiffness proportional damping model, the peak damping forces can be of a similar magnitude to the peak structural forces for systems with a high strength (low R) and high initial stiffness [28]. In such cases, the calculated results are likely to be unconservative, but there is not yet enough experimental evidence to determine how to accurately model inherent damping in self-centering systems. Therefore, this section examines how the results change if the initial damping model (Equation (2) with $k = k_1$) is replaced by the tangent damping model (Equation (3)). This reduces the damping forces when the SDOF system is in the nonlinear range, leading to larger displacements and thus a greater proportion of the results having a secant period that exceeds the ground motion filter cut-off of 10 s.

5.1. *Influence of initial period*

Figure 7 shows the variation of C_R with respect to initial period, T_1, when using the tangent damping model. Similar to the trends with the initial damping model, C_R decreases with T_1. However, compared with Figure 3, C_R is much larger, especially when T_1 is small. For example, in the case of $\beta = 50\%$ and $T_1 = 0.1$ s, $C_R = 16$ when $R = 2$ and $C_R = 130$ when $R = 4$, the latter of which corresponds to a drift of 3% for a 3.5 m tall one-storey structure. These values are much larger than the values of $C_R = 6.8$ and $C_R = 30$, respectively, that were calculated with the initial damping model. If the linear limit is further reduced to use $R = 8$, then $C_R = 214$ with the tangent damping model, meaning a drift of 5%. This suggests that, if the tangent damping model is more realistic than the initial damping model, it may be advisable to limit the response modification coefficient to small values (e.g. $R = 2$) for buildings with very short initial periods.

However, the value of C_R reduces rapidly as T_1 increases. For example, if $\beta = 50\%$ and $T_1 = 1.0$ s, $C_R = 1.7$ when $R = 4$, and $C_R = 3.8$ when $R = 15$. Despite these reductions, the only case where the equal displacement assumption is within 5% of accurate with the tangent damping model is when $R = 2, \beta = 100\%$ and $T_1 \geq 0.7$ s. The scale of Figure 7 makes it appear that C_R is close to 1 at long periods for $R = 2$ and $\beta = 50\%$,

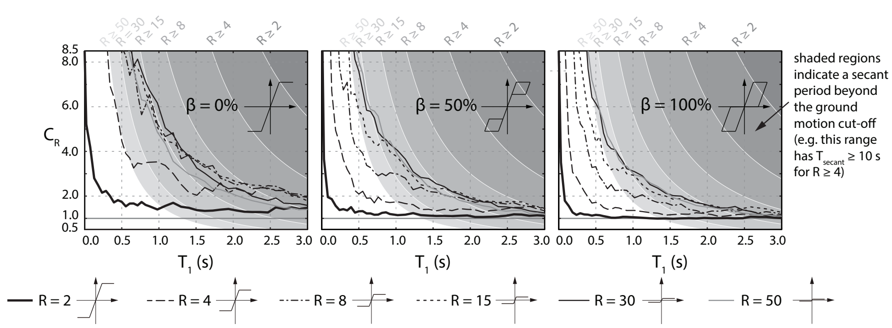

Figure 7: Displacement ratios of self-centering SDOF systems with respect to initial period with tangent damping model and $T_2 = \infty$.

but numerical results show that the equal displacement assumption underestimates C_R by more than 10%. For these cases where the secondary stiffness is zero ($T_2 = \infty$), the secant periods of the systems with $R = 8$ and $\beta = 0\%$ exceed the 10 s ground motion filter cutoff for $T_1 \geq 2.2$ s. When $R = 15$ or $R = 30$, this occurs for all $T_1 \geq 1.1$ s and $T_1 \geq 0.4$ s, respectively, while all of the results presented here for $R = 50$ caused the secant period to exceed 10 s.

5.2. Influence of response modification coefficient

Figure 8 shows the variation of C_R with respect to the response modification coefficient R with the tangent damping model. The shading indicates that, even for short initial periods, some of the results for systems with $R = 50$ cause T_{secant} to exceed 10 s if T_2 is large, and response modification coefficients as low as $R = 10$ can cause T_{secant} to exceed 10 s for long-period systems ($T_1 = 2.0$ s). Compared with the initial damping model, a similar trend of C_R increasing with R is observed when R is small, followed by a plateau or decrease above a critical R value. However, in addition to the values of C_R being much larger, especially at short initial periods, the distribution of curves with different β is more spread out when T_2 is large in Figure 8 than that in Figure 4. This indicates that the supplemental energy dissipation is more influential when the tangent damping model is used.

5.3. Influence of hysteretic energy dissipation

Figure 9 shows the variation of C_R with respect to β. Compared to the results with the initial damping model (Figure 5), the decrease in C_R with increasing β is stronger for small values of β. For example, in the case of $T_1 = 2.0$ s, $T_2 = \infty$ and $R = 4$, increasing β from 0% to 50% decreases C_R from 2.2 to 1.3, while further increasing β from 50% to 100% only reduces C_R to 1.2.

5.4. Influence of secondary period

The trends of C_R versus T_2 with the tangent damping model, shown in Figure 10, are generally similar to the trends with the initial damping model, although much larger displacement ratios are observed. However, because of the reduced inherent damping

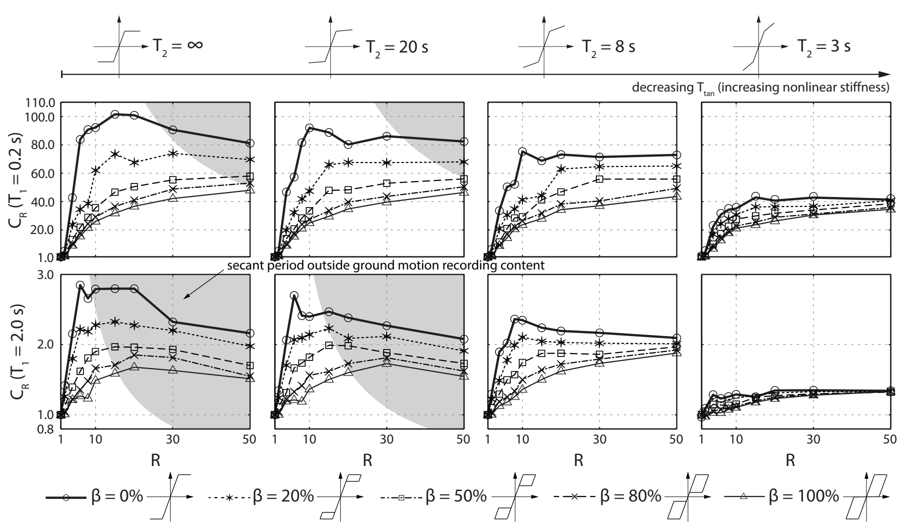

Figure 8: Displacement ratios of self-centering SDOF systems with respect to response modification coefficient with tangent damping model

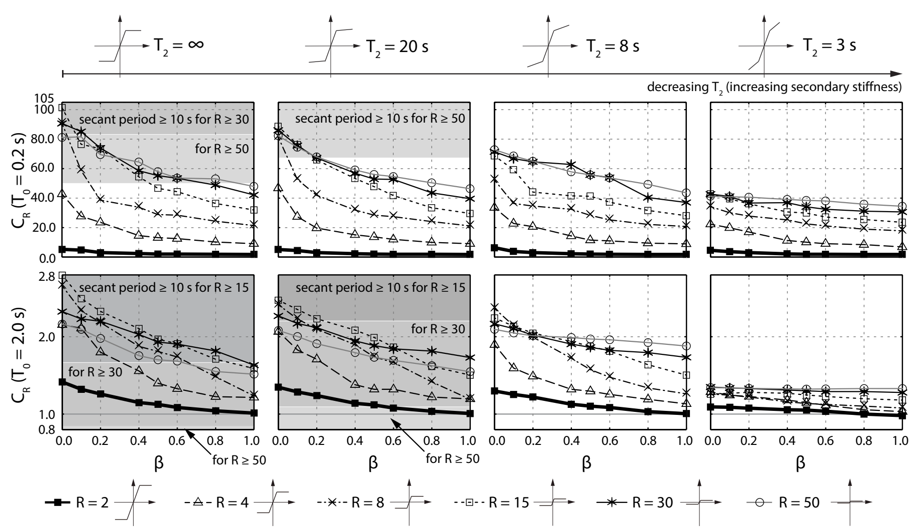

Figure 9: Displacement ratios of self-centering SDOF systems with respect to hysteretic energy dissipation parameter with tangent damping model

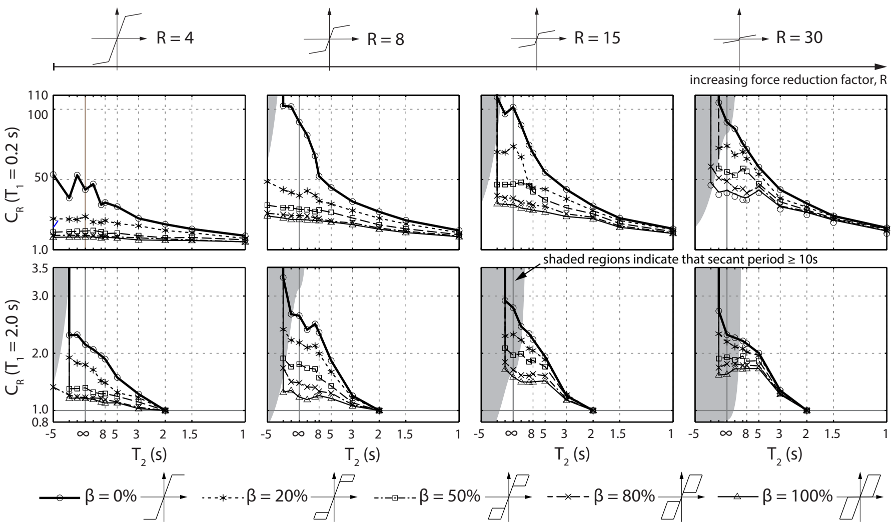

Figure 10: Displacement ratios of self-centering SDOF systems with respect to secondary period with tangent damping model

with the tangent damping model, the systems are more prone to dynamic instability. For example, in the case of $T_1 = 2.0$ s and $R = 4$, the system experiences dynamic instability for all considered values of β if the tangent damping model is adopted and T_2 = -5 s. By contrast, the system with the same properties does not experience dynamic instability if the initial damping model is adopted (see Figure 6). Another difference is that for long secondary periods (5 s $\leq T_2 \leq \infty$), Figure 10 shows a consistent decrease in C_R with increasing T_2 with the tangent damping model. Even if the slope does not appear to be much steeper than in Figure 6, the difference is not negligible because of the scale of vertical axis. For example, in the case of $T_1 = 0.2$ s, $R = 15$ and $\beta = 20\%$, the decrease in C_R when T_2 is changed from ∞ to 5 s is 40% with the tangent damping model, compared to 3% with the initial damping model. In other words, the post-tensioning is more effective in reducing displacements when the tangent damping model is assumed than it is when the initial damping model is assumed.

6. Regression Analysis

The discussion above demonstrated that the seismic displacement demand on a self-centering system is likely to exceed the equal displacement assumption. Therefore, there is a need for an equation that is simple enough to allow designers to quantify this effect without the need for nonlinear time history analysis. Seo [17] proposed an equation in the following form:

$$C_R = R^{\exp(f(\alpha,\beta,T_1))} \tag{10}$$

where

$$f(\alpha,\beta,T_1) = \frac{\left(a - b\sqrt{\alpha}\right)^2}{T_1^{\left(c-d\sqrt{\alpha}\right)^2}} - 1 \tag{11}$$

and a, b, c and d are regression coefficients that are tabulated for different values of β. This expression can be used to estimate the displacement demand in self-centering systems generally within an accuracy of 20% for the initial damping model for $1.5 \leq R \leq 8$ and $0\% \leq \beta \leq 50\%$ [17]. However, Zhang [28] has shown that Equation (10) does not extend beyond the range for which it was calibrated to capture the results of this study for large R values. Similarly, other recent proposals [18, 19] have not been calibrated for $R > 10$. In addition, a relatively simple expression is preferred for routine design.

To respond to these design needs, the results presented earlier are used to calibrate a new expression of the following form:

$$C_R = 1 + (R-1)^{b_1} \frac{b_2 + b_3(1-\beta)^{b_4}}{T_1^{b_5}} \tag{12}$$

where b_1, b_2, b_3, b_4 and b_5 are constants to be determined by regression for different damping models; these constants do not depend on any of the design parameters (i.e. R, β, or T) that define the hysteretic response of the SDOF system, as those parameters are included in the form of the regression equation. The form of the regression equation was selected because it includes all of the design parameters that define the hysteretic response of self-centering systems in a rational form except for T_2, which was shown to be the least significant parameter as long as it is positive and not close to the initial period. Reducing T_2 generally reduces C_R, so it is conservative to consider only $T_2 = \infty$

in the regression analysis. Based on general observations from the SDOF analyses, the displacement ratios are proportional to both R and $1-\beta$, and inversely proportional to the initial period T_1. The equation is also physically consistent in that it returns a lower-bound value of 1 for $R = 1$ (i.e. if the system were elastic). Formulating the regression equation in this way will also make it simple to apply for routine design purposes.

Only $4 \leq R \leq 30$ are considered in the regression because $R = 50$ is likely to reduce the seismic design loads to less those from wind design loads in many cases and is therefore unlikely to be a practical value, and because it frequently led to a secant period that was longer than the 10 s cut-off of the ground motion filter. Although some of the results for $R = 30$ also led to a secant period beyond 10 s, the trends of the data in this region were still similar to the trends for other parameters that did not cause the secant period to exceed the ground motion filter cut-off period. Conversely, a response modification coefficient of $R = 2$ is not included because it is considered too small to take advantage of the benefits of a self-centering system for which the nonlinear displacements are not the result of structural damage. One of the primary motivations behind selecting a self-centering system is the ability to significantly reduce the seismic design loads and resulting member sizes without compromising on the performance of the structure.

The results with $\beta \leq 10\%$ are also not considered in the regression because they tended to dominate the regression and because most design proposals for self-centering systems recommend including hysteretic energy dissipation (e.g. [8, 33]). Even for these cases that are not included in the regression, the applicability of Equation (12) will still be checked.

Potential regression coefficients were evaluated based on the residual, which was calculated using Equation (13):

$$Residual = \frac{C_{R,predicted} - C_{R,observed}}{C_{R,observed}} \tag{13}$$

By this definition, a positive residual means that the equation conservatively overestimates the displacement and a negative residual means that it unconservatively underestimates the displacement.

Table 2: Coefficients from regression analyses

Damping model	b_1	b_2	b_3	b_4	b_5	Root Mean Squared Error of Residual
initial	0.515	0.184	0.119	1.173	1.478	10%
tangent	0.630	0.292	0.477	1.697	1.567	16%

The ”fitnln” function in Matlab [26] was used to minimize the absolute value of *Residual*, using an iterative generalized least squares algorithm to fit the nonlinear regression model. The coefficients from the regression are summarized in Table 2. Using the coefficients from Table 2, the residuals are calculated using Equation (13) and plotted in Figure 11. For the regression equation developed for the initial damping model, the residuals are accurate to within 20% in most cases. The accuracy is similar for all values of $0\% \leq \beta \leq 100\%$. However, the equation tends to slightly underestimate the displacement ratio when $T_1 \leq 0.3$ s, and to underestimate the displacement ratio by up to 70% in the range of T_1 for which it was not calibrated ($T_1 \leq 0.15$ s). The regression equation developed for the tangent damping model tends to have larger errors than for the initial damping model, but is still generally accurate to within 30% for $\beta \geq 20\%$. The displacement estimates are very conservative for β =0%, and as was the case with the initial damping model, they are very unconservative for periods that were excluded from the regression analysis ($T_1 \leq 0.15$ s). Overall, although this expression is not exact, it provides a simple way to estimate the displacements to within a reasonable degree of accuracy for routine design.

Figure 12 shows the residuals from the same equation for a high secondary stiffness ($T_2 = 3$ s instead of $T_2 = \infty$). For the initial damping model, the residuals shift upwards by about 0.2, making almost all results conservative. However, the regression equation is still accurate to within approximately 30% in most cases. For the tangent damping model, the regression equation tends to overestimate the displacements, with the degree of overestimation increasing as β reduces. None of the residuals falls below 0 for any $T_1 \geq 0.2$ s. Even if it is very conservative to use the regression equation with the tangent damping model for this value of T_2, the estimates are still within about 30% with $R \leq 15$ and $\beta \geq 80\%$.

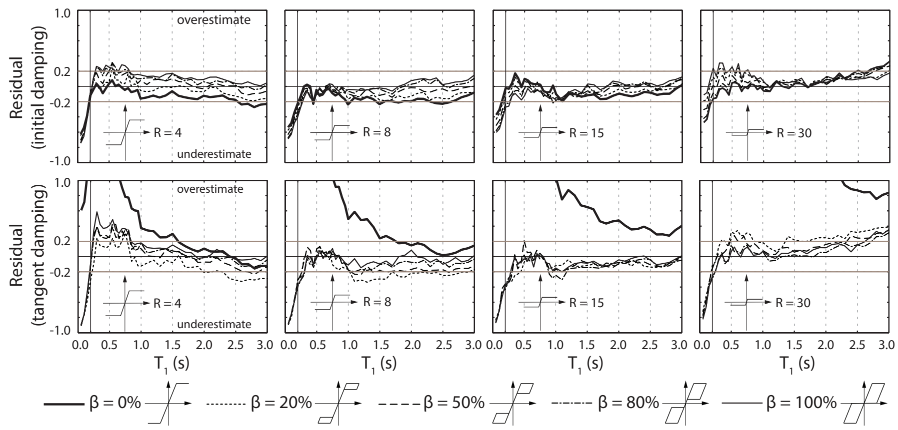

Figure 11: Relative error between predicted and observed displacement demands with $T_2 = \infty$

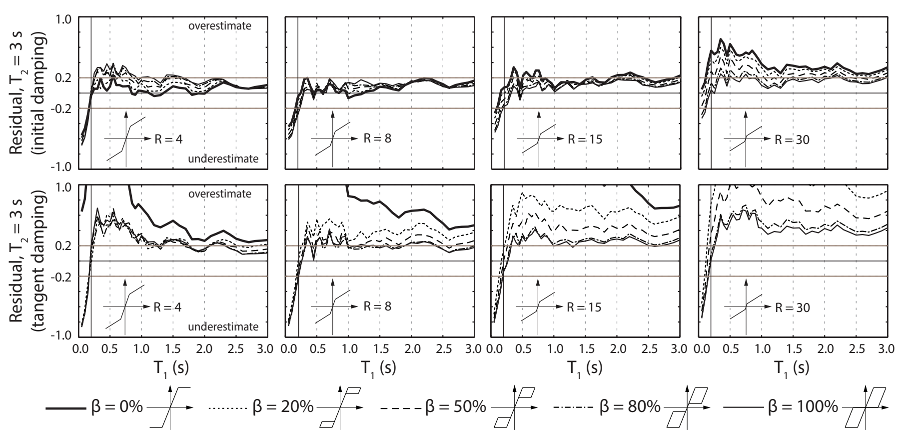

Figure 12: Relative error between predicted and observed displacement demands with $T_2 = 3$ s

7. Example applications

To highlight the physical significance of several of the parameters selected for the parametric study, and to demonstrate the application of the above regression equation, this section considers four example controlled rocking steel braced frames (Figure 1(c)). Controlled rocking steel braced frames are chosen because their displacements are generally dominated by the first-mode response, particularly for shorter buildings, if the frame members are designed to remain elastic and the nonlinear mechanism is rocking at the base only (e.g. [9, 34]).

7.1. Design of the self-centering nonlinear mechanism

Controlled rocking steel braced frames were designed for three-storey, six-storey and nine-storey buildings; one design case was considered for the three-storey and nine-storey buildings, and two design cases were considered for the six-storey building. All of the buildings have a first-storey height of 4.2 m, and a storey height above the first storey of 3.8 m. Each floor has a seismic weight of 10 200 kN, and the roof has a seismic weight of 6430 kN. The floor plan is 48 m by 32 m, with 8 m bays in each direction. The structures are located on a site in Los Angeles with Site Class D as defined in ASCE 7 [22], with a short-period design-level spectral acceleration of $S_{DS} = 1.0$ g and a one-second period design-level spectral acceleration of $S_{D1} = 0.6$ g. The fundamental periods of the three-storey, six-storey and nine-storey buildings were determined to be 0.4 s, 0.7 s, and 1.3 s using modal analysis of elastic frame models for the buildings, in which the frame members were capacity designed using the dynamic procedure proposed by Steele and Wiebe [34]. In the dynamic procedure, the capacity design forces are computed by taking the frame member forces under the maximum post-tensioning force, maximum energy dissipation force, and equivalent static forces calculated using the design code (e.g. ASCE 7 [22]) and combining them with those computed for the elastic higher modes through a modal response spectrum analysis; an elastic rocking model is used where the boundary conditions reflect the response of the frame in the secondary stiffness range.

The values of R and β were chosen to limit the predicted peak seismic displacements of each building to 2.5%. For the three-storey structure, the design parameters were selected to be $R = 20$ and $\beta = 90\%$ with two frames in each direction. The design base shear was calculated to be 670 kN per frame, which was distributed along the height of the building using the equivalent static procedure [22]. The post-tensioning, which was anchored at the top in the centre of the frame, was designed with a prestress equal to 20% of the ultimate stress. This required 16 post-tensioning strands, as opposed to 39 that would have been required for a design with $R = 8$. Designing with $R = 20$ instead of $R = 8$ also reduced the activation force of the supplementary energy dissipation from 900 kN to 360 kN. Based on the post-tensioning and energy dissipation design parameters selected, the secondary period of the three-storey controlled rocking steel braced frame was $T_2 = 3$ s.

For the six-storey building, two different design cases were considered: in the first, the post-tensioning was anchored at the top of both columns of the frames, while in the second, the post-tensioning was anchored at the top centre of the frames. Both cases were designed with parameters of $R = 30$ and $\beta = 70\%$, with four frames in each direction. Seismic loading governed the design of the lateral force limiting mechanism over wind loading, despite using such a large value for R. The design base shear was calculated to be 412 kN per frame for both cases, because the initial periods and response modification coefficients were the same for both. The post-tensioning prestress was selected to be 25% of the ultimate stress for both cases in the six-storey building. For the first case, in which the post-tensioning was anchored at the top of both columns of the frames, the secondary period was calculated to be $T_2 = 5$ s. For the second case, in which the post-tensioning was anchored at the top-centre of the frames, the secondary period was determined to be $T_2 = 27$ s. Unlike conventional lateral force resisting systems, in which the secondary stiffness is defined by the nonlinear material properties of the frame members, the six-storey designs highlight how the secondary stiffness of a self-centering system can be substantially different even when the initial period is the same. Both designs with $R = 30$ required 28% of the number of post-tensioning strands that would have been required using $R = 8$, and they also reduced the activation force of the supplementary energy dissipation from 1210 kN to 320 kN.

Finally, for the nine-storey building, the design parameters were chosen to be $R = 15$ and $\beta = 0\%$ (i.e. no hysteretic energy dissipation) with four frames in each direction. The design base shear was calculated to be 675 kN per frame. The 27 post-tensioning strands were anchored at the top, centre of the frame, and were designed using a prestress of 50% of the ultimate stress. A design using $R = 8$ would have required 51 strands. The secondary period of the frame with these design parameters is T_2 = -15 s. This design is a possible realisation given the flexibility of the design parameter selection. This case is used as an example for when the regression equation for C_R is not expected to provide accurate estimates of the nonlinear displacements because the tangent period is negative and the energy dissipation ratio is zero. This design case is intended to contrast with the three other design examples for which the parameters are within the range of calibration.

Figure 13 shows the push-pull hystereses for all of the controlled rocking steel braced frames, from which the roof displacements at the onset of rocking (Δ_y) for the three-storey, both six-storey and nine-storey frames were determined to be 0.0288%, 0.0300%, and 0.0792% of the building height, respectively.

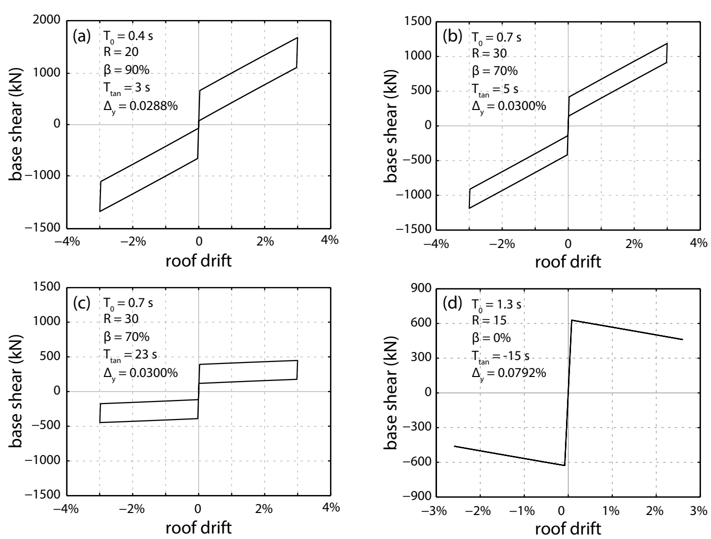

Figure 13: Push-pull response for the a) three-storey, b) six-storey (case 1), c) six-storey (case 2), and d) nine-storey example frames to 3.0% roof drift

7.2. Application of the regression equation

In this subsection, Equation 12 is used to estimate the peak interstorey drifts of the four example designs. The rocking displacements (Δ_y) of each frame in Figure 13 are then multiplied by the response modification coefficients to calculate the displacement of the equivalent linear system. As C_R is a ratio of the maximum displacement of the self-centering system to the maximum displacement of the equivalent linear system, the peak roof-level displacement in each structure can be calculated as:

$$\Delta_{max,est} = C_R \times \Delta_{max,elastic} = C_R \times R\Delta_y \tag{14}$$

All of the example controlled rocking steel braced frames were analysed in OpenSees [35] using the same model developed by Steele and Wiebe [36] except that the post-tensioning was modelled using a linear elastic material model. The post-tensioning was included as a corotational truss element, and the linear elastic material model was wrapped in an initial stress material to include the prestress. The frame members were all modelled as linear elastic with and elastic modulus of 200 GPa. Gap elements (compression only) were included at the base of the frame to model column uplift and the transfer of base shear. A leaning column was included to account for the reduced stiffness from the P-Delta effects; the leaning column was modelled using elastic beam column elements with an axial stiffness representative of the gravity columns tributary to the frame, and negligible flexural stiffness to avoid any contribution to resisting lateral loads. Initial stiffness proportional Rayleigh damping applied to all elements except for the gap elements at the base that were used to model the rocking behaviour. Further discussion on the numerical model is available in [36].

The same ground motions discussed in Section 3 were used for the analysis, with a scaling factor of 2.17 to match the median response spectrum to the design basis earthquake (DBE) elastic design spectrum for Los Angeles for periods between 0.2 and 2.0 s, such that the same ground motion scaling could be used for all example frames. Table 3 summarises the design parameters and shows the rocking displacement, Δ_y, the displacement ratio, C_R, the corresponding estimates of the estimated median peak displacement, $\Delta_{max,est}$, and the median peak displacement for each frame from the non-linear time history analysis, Δ_{max}.

All of the SDOF results were based on the initial damping model, so as to be consistent with the mass-proportional term in the Rayleigh damping that dominates the first-mode damping in the MDOF model. Using the tangent damping model would have increased the predicted displacements of the three- , six-, and nine-storey structures to 5.24%, 5.55%, and 4.38%, respectively, which would not have satisfied the design intent. This underscores the importance of the assumed inherent damping model, not only in these SDOF analyses, but also in more detailed analyses of MDOF systems.

7.3. Comparison of predicted displacements with analysis results

For the three-storey frame, the predicted nonlinear displacement of 2.53% at the DBE level was only slightly more than the median peak roof drift of the three-storey frame from the nonlinear time history analysis of 2.50%. Also, the peak roof drift and the peak interstorey drift were nearly identical. Referring to Figure 12, the accurate estimates would have been expected, because the residual is very close to zero for the set of parameters used in this example design.

For the two six-storey frames, Equation (12) predicted the nonlinear displacements as 2.74% for both frames, compared to median peak roof drifts from the nonlinear time history analysis results of 2.41% and 2.51%. This error of less than 13% was consistent with what was expected from the calibration of Equation (12) for the initial damping model with similar system parameters. As expected based on the SDOF analyses, the displacements in both systems were very similar to one another, despite the differences in secondary period.

For the nine-storey frame, the peak roof drift was estimated to be 2.14%, which was 26% less than the median peak roof drift of 2.90% from the nonlinear time history

Table 3: Design parameters for the controlled rocking steel braced frame buildings

Design	T_1	R	β	T_2	Δ_y*	C_R	$\Delta_{max,est}$*	Δ_{max}*
three-storey	0.4 s	20	90%	3 s	0.0288%	4.39	2.53%	2.50%
six-storey (case 1)	0.7 s	30	70%	5 s	0.0300%	3.04	2.74%	2.41%
six-storey (case 2)	0.7 s	30	70%	27 s	0.0300%	3.04	2.74%	2.51%
nine-storey	1.3 s	15	0%	-15 s	0.0792%	1.80	2.14%	2.90%

*All Δ values are expressed as a percentage of the roof-level displacement to the building height analysis; this is outside the range of the residual error of the regression equation. In addition to the negative residual error of 12% for this set of design parameters, this underestimation was likely due to a combination of the nine-storey frame having a negative secondary stiffness, which was shown to result in larger displacements in the SDOF analyses, and also the more flexible frame having more significant higher mode response, which is not captured in the SDOF analyses. Nevertheless, this error was considered acceptable for preliminary design, particularly considering the simplicity of the regression equation.

8. Conclusions

This paper presented a parametric study on the seismic displacements of self-centering systems on stiff soil sites under broadband ground motions, with particular attention to systems with low linear limits (large R) or negative secondary stiffness ($k_2 < 0$), and including both initial and tangent stiffness proportional damping models. The results were presented using constant-strength spectra that show the peak displacement ratios for self-centering and linear systems with the same initial period. Although this displacement ratio (C_R) was very large at short initial periods (e.g. $T_1 \leq 0.5$ s), the actual displacement may still be within acceptable limits, and C_R approached unity as the period increased. Reducing the linear limit (i.e. increasing R) significantly increases the peak displacement when the response modification coefficient is small ($R \leq 8$), but as R or T_1 increases, further increases in R cause less significant increases to the peak displacement. Increasing the hysteretic energy dissipation from no hysteretic energy dissipation ($\beta = 0\%$) to the maximum self-centering hysteretic energy dissipation ($\beta = 100\%$) generally reduces the peak displacements by up to 50%, but the influence of increasing β diminishes as β approaches 100%, and is less for systems with long periods. If the secondary stiffness is positive but small, it has little effect. However, if it becomes negative due to P-Delta effects, the response can become unbounded when R or T_1 is large, and this dynamic instability is not prevented by increasing the hysteretic energy dissipation. Therefore, it is not recommended to design self-centering structures with these properties.

The general trends of variation of C_R with respect to different hysteretic parameters are the same regardless of which damping model is used, but the tangent damping model results in larger peak displacements and increased susceptibility to dynamic instability when the secondary stiffness is negative. With the tangent damping model, the reductions in displacement demands with increasing supplemental energy dissipation and secondary stiffness are more pronounced. More experimental data are needed to determine how best to model inherent damping in self-centering systems.

Based on these SDOF analyses, an empirical equation was developed for the displacement ratio C_R as a function of T_1, R, and β, and was calibrated for both the initial damping model and the tangent damping model. Four example controlled rocking steel braced frames were designed, demonstrating the potential benefits of using large values of R. The proposed regression equation was shown to be almost exact when compared to the results of nonlinear time history analyses for the three-storey building, for which the roof displacements were dominated by the first mode. The equation became less precise with increasing building height, with errors of up to 13% for the six-storey buildings and 26% for the nine-storey building. However, considering the importance of quantifying the increase in displacements of self-centering systems relative to the equal displacement assumption, the proposed equation was considered to achieve a balance between simplicity and accuracy that was appropriate for routine design.

Given that the analyses presented in this study were all for a set of ground motions that represents a site with stiff soil conditions, the application of the regression equation presented here should be limited to such sites. A separate ground motion set representing rock sites has been used and achieved similar results [28]. It is expected that the equations presented here would be unconservative for sites with softer soil conditions (i.e. ASCE 7 site classes E and F) because of the relatively higher low-frequency content. New regression equation coefficients could be computed for such sites using the methodology presented in this study.

Acknowledgements

The financial support from the Department of Civil Engineering, McMaster University is greatly appreciated.

References

References

[1] W. Kam, S. Pampanin, R. Dhakal, H. Gavin, C. Roeder, Seismic performance of reinforced concrete buildings in the September 2010 Darfield (Cantebury) Earthquake, Bulletin of the New Zealand Society for Earthquake Engineering 43 (2010) 340–350.

[2] C. Clifton, M. Bruneau, G. Macrae, R. Leon, A. Fussell, Steel structures damage from the Christchurch Earthquake series of 2010 and 2011, Bulletin of the New Zealand Society for Earthquake Engineering 44 (2011) 298–318.

[3] Y. Iwata, H. Sugimoto, H. Kuwamura, Reparability limit of steel structural buildings based on the actual data of the Hyogoken-Nanbu Earthquake, Journal of Structural and Construction Engineering: Transactions of AIJ 588 (2005) 165–172.

[4] J. McCormick, H. Abrano, M. Ikenaga, M. Nakashima, Permissible residual deformation levels for building structures considering both saftety and human elements, in: 14th World Conference on Earthquake Engineering, Beijing, China, 2008.

[5] M. Priestley, S. Sritharan, J. Conley, P. S., Preliminary results and conclusions from the PRESSS five-story precast concrete test building, PCI Journal 44 (1999) 42–67.

[6] Y. Kurama, S. Pessiki, R. Sause, L.-W. Lu, Seismic behaviour and design of unbonded post-tensioned precast concrete walls, PCI Journal 44 (2010) 72–89.

[7] D. Roke, R. Sause, J. Ricles, C.-Y. Seo, K.-S. Lee, self-centering seismic-resistant steel concentrically-braced frames, in: 8th U.S. National Conference on Earthquake Engineering, San Francisco, CA, 2006.

[8] M. R. Eatherton, X. Ma, H. Krawinkler, D. Mar, S. Billington, J. Hajjar, G. Deierlein, Design concepts for controlled rocking of self-centering steel-braced frames, Journal of Structural Engineering 140 (2014) 4014082 1–10.

[9] L. Wiebe, C. Christopoulos, R. Tremblay, M. Leclerc, Mechanisms to limit higher mode effects in a controlled rocking steel frame. 1: Concept, modelling, and low-amplitude shake table testing, Earthquake Engineering & Structural Dynamics 42 (2013) 1053–1068.

[10] L. Wiebe, C. Christopoulos, R. Tremblay, M. Leclerc, Mechanisms to limit higher mode effects in a controlled rocking steel frame. 2: Concept, modelling, and low-amplitude shake table testing, Earthquake Engineering & Structural Dynamics 42 (2013) 1069–1086.

[11] C. Christopoulos, R. Tremblay, H. Kim, M. Lacerte, Self-centering energy dissipative bracing system for the seismic resistance of structures: Development and validation, Journal of Structural Engineering 134 (2008) 96–107.

[12] J. Erochko, C. Christopoulos, R. Tremblay, H.-J. Kim, Shake table testing and numerical simulation of a self-centering energy dissipative braced frame, Earthquake Engineering & Structural Dynamics 42 (2013) 1617–1635.

[13] R. DesRoches, B. Smith, Shape memory alloys in seismic resistant design and retrofit: A critical review of their potential and limitations, Journal of Earthquake Engineering 8 (2004) 415–426.

[14] L. Wiebe, C. Christopoulos, Performance-based seismic design of controlled rocking steel braced frames. I: Methodological framework and design of base rocking joint, Journal of Structural Engineering 141 (2014) 04014226 1–10.

[15] C. Christopoulos, A. Filiatrault, B. Folz, Seismic response of self-centering hysteretic SDOF systems, Earthquake Engineering & Structural Dynamics 31 (20102) 1131–1150.

[16] C.-Y. Seo, R. Sause, Ductility demands on self-centering systems under earthquake loading, ACI Structural Journal 102 (2005) 275–285.

[17] C.-Y. Seo, Influence of Ground Motion Characteristics and Structural Parameters on Seismic Responses of SDOF Systems, Ph.D. thesis, Lehigh University, Bethlehem, PA, 2005.

[18] N. Rahgozar, A. Moghadam, A. Aziminejad, Inelastic displacement ratios of fully self-centering controlled rocking systems subjected to near-source pulse-like ground motions, Engineering Structures 108 (2016) 113–133.

[19] A. Joó, A. Zsarnoczay, M. Opoldusz, L. Kollar, Applicability of modal response spectrum analysis on rocking structures, in: 16th World Conference on Earthquake Engineering, Santiago, Chile, 2017.

[20] M. Priestley, D. Grant, Viscous damping in seismic design and analysis, Journal of Earthquake Engineering 9 (2005) 229–255.

[21] P. Charney, Unintended consequences of modeling damping in structures, Journal of Structural Engineering 143 (2008) 581592.

[22] American Society of Civil Engineers (ASCE), Minimum design loads for buildings and other structures, ASCE/SEI Standard 7-16, American Society of Civil Egnineers, Reston, VA, United States, 2016.

[23] E. Miranda, Inelastic displacement ratios for structures on firm sites, Journal of Structural Engineering 126 (2000) 1150–1159.

[24] L. Wiebe, C. Christopoulos, A cantilever beam analogy for quantifying higher mode effects in multistorey buildings, Earthquake Engineering & Structural Dynamics 44 (2015) 1697–1716.

[25] L. Wiebe, C. Christopoulos, R. Tremblay, M. Leclerc, Modelling inherent damping for rocking systems: results of large-scale shake table testing, in: 15th World Conference on Earthquake Engineering, Lisbon, Portugal, 2012.

[26] MATLAB version 8.4.0 (R2014b) student version, The Mathworks, Inc., Natick, Massachusetts, 2014.

[27] A. Chopra, Dynamics of structures: theory and application to earthquake engineering, 4th ed., Prentice Hall, 2012.

[28] C. Zhang, Seismic displacement demands on self-centering single-degree-of-freedom systems, Master's thesis, McMaster University, Hamilton, ON, Canada, 2015.

[29] J. W. Baker, T. Lin, S. K. Shahi, New ground motion selection procedures and selected motions for the PEER transportation research program, PEER Report 3011/03, Pacific Earthquake Engineering Research Center, University of Califonia, Berkeley, 2011.

[30] Pacific Earthquake Engineering Research Center (PEER), Ground motion studies for transportation systems, 2011. Available from: http://peer.berkeley.edu/transportation/projects/ground-motion-studies-for-transportation-systems/.

[31] D. Ancheta, B. Darragh, P. Stewart, E. Seyhan, W. Silva, S. Chiou, E. Wooddell, W. Graves, R. Kottke, M. Boore, T. Kishida, L. Donahue, PEER NGA-West2 Database, PEER Report 2013/03, Pacific Earthquake Engineering Research Center, University of Califonia, Berkeley, 2013.

[32] Applied Technology Council, Effects of strength and stiffness degradation on seismic response, FEMA Report 440A, Federal Emergency Management Agency, Washington, D.C., United States, 2009.

[33] L. Wiebe, G. Sidwell, S. Gledhill, Design guide for controlled rocking steel braced frames, Report SCNZ 110, Steel Construction New Zealand, Manukau City, New Zealand, 2015.

[34] T. Steele, L. Wiebe, Dynamic and equivalent static procedures for capacity design of controlled rocking steel braced frames, Earthquake Engineering & Structural Dynamics 45 (2016) 2349–2369.

[35] OpenSees, Open system for earthquake engineering simulation v2.4.5 [computer software], 2015.

[36] T. Steele, L. Wiebe, Collapse risk of controlled rocking steel braced frames with different post-tensioing and energy dissipation designs, Earthquake Engineering & Structural Dynamics 46 (2017) 2063–2082.